Eur. Phys. J. D **35**, 3–14 (2005)
DOI: 10.1140/epjd/e2005-00198-1

THE EUROPEAN PHYSICAL JOURNAL D

Manipulating atoms and molecules with evanescent-wave mirrors

S. Kallush[1], B. Segev[1,a], and R. Côté[2,b]

[1] Department of Chemistry, Ben-Gurion University of the Negev, Beer-Sheva 84105, Israel
[2] Physics Department, University of Connecticut, 2152 Hillside Road, Storrs, Connecticut 06269, USA

Received 31 March 2005 / Received in final form 11 May 2005
Published online 26 July 2005 –

Abstract. We explore how atoms and polar molecules can be manipulated using evanescent-wave mirrors (EWM). We review the simpler case of ultracold atoms incident on EWM, and show that quantum effects such as tunneling, above barrier reflection, and Casimir retardation corrections, can be probed. We show that it is possible to enhance significantly quantum effects by engineering sharp features in the effective atom-EWM potential. We illustrate the concept with a bichromatic EWM created by using red and blue detuned lasers. Finally, we extend the treatment to ultracold diatomic polar molecules. Quantum reflection and molecular state selection are demonstrated under attainable physical conditions. By facilitating the manipulation and trapping of ultracold molecules, such molecular mirrors could have several applications, e.g., as devices to filter and select state for ultracold chemistry, or to manipulate states for quantum information processing.

PACS. 33.80.-b Photon interactions with molecules – 42.50.-p Quantum optics

1 Introduction

Evanescent-wave mirrors (EWMs) have been used as a tool for examining fundamental effects in quantum mechanics. In addition to quantum reflection and tunneling of ultracold atoms [1–4], fundamental types of interactions, such as the classical van der Waals atom-wall potential or QED retardation effects [5–7] have been studied. These devices have also been utilized in various applications, such as gravito-optical traps for ultracold atoms [8]. Molecular EWMs are just starting to be investigated; they have been first prepared in [9], and quantum state selection by molecular EWMs was also implemented in [10]. Recently, Schulz et al. [11] presented the possibility of miniature molecular EWMs. Such devices could serve as components in quantum computers based on polar molecules [12].

The recent advances in producing and trapping of ultracold molecules via various techniques, such as photoassociation [13–16], buffer-gas thermalization [17,18], and Stark decelerator [19–21], have opened the way to study molecules in the few μK regime [13–16]. In that temperature regime, the kinetic energy of ultracold molecules is comparable with the energy of the molecule-wall interaction. Hence, one could use ultracold molecules to measure the molecule-wall long-range interaction, as was done in the case of atoms [5,6].

In this paper, we first review EWMs for atoms under realistic physical conditions. We explore the reflection probability for a "monochromatic" atomic EWM with and without retardation effects, and investigate more complicated interaction potentials created, e.g., with a "bichromatic" atomic EWM. We then present a description of the interaction for a molecular EWM. We consider ultracold polar diatomic molecules, and show that the light field of the EWM couples internal molecular states, so that quantum reflection from such devices can lead to quantum state selection.

2 Atoms

An evanescent-wave mirror for cold atoms is created when a blue-detuned laser beam undergoes total internal reflection inside a dielectric prism [1,2]. The effective potential acting on the atom combines two contributions: the optical potential originating from the evanescent optical field, and the atom-wall interaction (see Fig. 1).

2.1 Optical potential

Optical potentials are induced by space dependent changes to the internal energy of the atoms. A simple model for a two level atom was given within the dressed atom approach [22]. By solving the optical Bloch equations in the electric dipole approximation, one finds two

[a] This publication is dedicated to our friend and colleague, Bilha Segev, who passed away on March 17, 2005. She will be missed by her friends, colleagues, and the physics and chemistry communities.

[b] e-mail: rcote@phys.uconn.edu

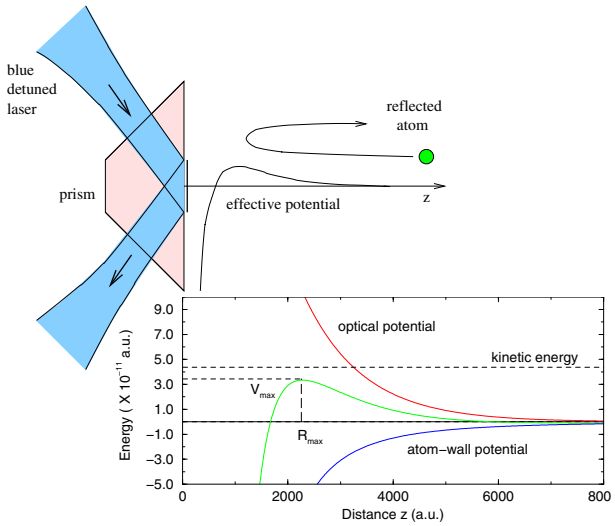

Fig. 1. Schematic of an atomic mirror. The blue detuned laser light produces a repulsive force, after total internal reflection. An approaching atom will feel the effective potential formed by the atom-wall and light induced potentials. The lower panel shows the contributions to the effective potential for Na atoms.

forces acting on an atom in its ground state: a radiation pressure force and a dipole force [22]. The dipole force can be described by the effective potential

$$V_{\rm dipole} = \frac{\hbar\delta}{2} \ln\left[1 + \frac{\Omega^2/2}{\delta^2 + \Gamma^2/4}\right], \qquad (1)$$

where Ω is the Rabi frequency, and $\delta \equiv \omega_L - \vec{k}_L \cdot \vec{p} - \omega_0$ is the detuning from the atomic resonance of frequency ω_0 and natural linewidth Γ of an atom of momentum $\vec{p}$ interacting with photons of momentum $\vec{k}_L$ and frequency ω_L. For large δ, the dipole force dominates [22] and $V_{\rm dipole}$ reduces to

$$V_{\rm dipole} \overset{\text{large } \delta}{\longrightarrow} \frac{\hbar\Omega^2}{4\delta}, \qquad (2)$$

with $\Omega^2 \propto Id^2$ where I is the laser intensity and d is the atomic dipole. The dipole potential is therefore proportional to the intensity of the laser and inversely proportional to detuning, and can be attractive or repulsive, according to the sign of δ. For red detuning $\omega_L < \omega_0$, $\delta < 0$, and the atom is attracted by high intensity, while for blue detuning, $\omega_L > \omega_0$, $\delta > 0$, it is repelled by high intensity.

2.2 Atom-dielectric interaction with and without retardation effects

A simple model for the interaction of a ground state atom and a wall of dielectric constant ϵ considers the interaction between a dipole $\vec{d}$ and its mirror image. It gives the Lennard-Jones potential

$$V_{\rm LJ} = -\left(\frac{\epsilon - 1}{\epsilon + 1}\right)\left(\frac{\langle d_{||}^2\rangle + 2\langle d_{\perp}^2\rangle}{64\pi\epsilon_0}\right) z^{-3} = -\frac{C_3}{z^3}, \qquad (3)$$

Table 1. Parameters for sodium used in this paper. The values of $C_3^{\rm metal}$ and $K_4^{\rm metal}$ are taken from Karchenko et al. [26], and K_4 is from [27].

parameter	value
n	1.805
k_L	5.645×10^{-4} a.u.
θ	45°
κ	4.4771×10^{-4} a.u.
$C_3^{\rm metal}$	1.889 a.u.
$K_4^{\rm metal}$	2676.71 a.u.
K_4	1081.03 a.u.
m	41907.782 a.u.

where $\langle d_{||}^2\rangle$ and $\langle d_{\perp}^2\rangle$ are the expectation values of the squared dipole parallel and perpendicular to the surface [23], $\epsilon = n^2$ and n is the index of refraction of the dielectric. This expression for the potential is approximately valid for constant ϵ and small z. C_3 is related to the constant $C_3^{\rm metal}$ of a pure metallic wall by $C_3 = C_3^{\rm metal}(n^2 - 1)/(n^2 + 1)$. The numerical values for Na atoms used in this paper are given in Table 1.

If we take into account retardation effects, the Casimir-Polder potential is obtained where the finite propagation time between the dipole and its image results in a different asymptotic power-law behavior; $V(z) \propto z^{-4}$ as $z \to \infty$ [24]. The complete QED treatment depends on the dynamic dipole polarizability function [25], and gives

$$V_{\rm QED}(z) = -f(z)\frac{C_3}{z^4}, \qquad (4)$$

where $f(z) \to z$ for small z and $f(z) \to K_4/C_3$ for $z \to \infty$. Using semi-empirical results for the dynamic dipole polarizability, accurate QED potential curves were obtained for alkali atoms [26].

2.3 Effective potential of the evanescent-wave mirror

An evanescent-wave mirror for cold atoms is created when a blue-detuned laser beam ($\delta > 0$) with wave number $\vec{k}_L$ undergoes total internal reflection inside a dielectric prism. The effective potential felt by an approaching atom is simply the sum of $V_{\rm optical}$ and $V_{\rm wall}$. Because the laser intensity drops exponentially with the distance z outside the surface of the dielectric prism, we have

$$V_{\rm optical} = C_0 \exp(-2\kappa z) \exp(-\rho^2/\rho_0^2), \qquad (5)$$

where $\kappa = k_L\sqrt{n^2 \sin^2\theta - 1}$, and the incident angle is θ. For large detuning [28], $C_0 \simeq Id^2/8\hbar\epsilon_0\delta$, where d is the atomic dipole moment, and ϵ_0 the vacuum permittivity. The $\exp(-\rho^2/\rho_0^2)$ factor accounts for the Gaussian profile of the focused laser beam of width ρ_0. We have shown in reference [29] that this Gaussian profile needs to be considered when analyzing experimental results. However, we assume a constant intensity and set $\rho^2 = 0$ for simplicity.

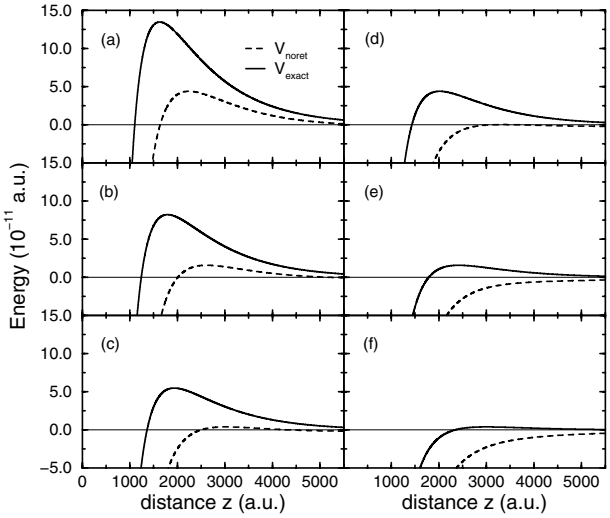

Fig. 2. The effective potential with retardation $V_{\rm exact}$ (solid line) and without retardation $V_{\rm noret}$ (dashed line) as a function of z for various values of C_0. As C_0 decreases from (a) to (f), the barrier diminishes and is pushed out. Notice that for (e) and (f), there is no barrier for $V_{\rm noret}$. The corresponding numerical values are listed in Table 2.

The exponentially decaying optical potential and the attractive atom-wall interaction add up to generate an effective potential barrier. It is given by one of the following two formulas, which, respectively, neglect retardation effects or take them into account [30],

$$V_{\rm noret}(z) = C_0 \exp(-2\kappa z) - \frac{C_3}{z^3}, \qquad (6)$$

$$V_{\rm exact}(z) = C_0 \exp(-2\kappa z) + V_{\rm QED}(z)\ . \qquad (7)$$

The height of the barrier $V_{\rm max}$ varies as a function of the intensity of the laser beam, as do its location and shape. This is illustrated in Figure 2, where we used the various numerical values listed in Table 1. As I is reduced, $V_{\rm max}$ decreases and moves out to larger distances. For $V_{\rm max} = \frac{1}{2}mv_{\rm top}^2$ corresponding to sodium atoms with $v_{\rm top} = 10.0$ cm/s, the top of the barrier is located at a distance of roughly $2000a_0$, i.e. far out from the prism itself. This enable us to treat the system without taking into account many surface phenomena, e.g. the sticking of the atoms to the surface, the creation of phonons, etc. At such large distances, retardation effects could be noticeable. Indeed, when z becomes of the order of the transition wavelength $\lambda/2\pi$, the time-of-flight of the virtual photons becomes large enough to cause retardation effects. For sodium, $\lambda/2\pi = 1772a_0$, and a barrier located at $2000a_0$ could probe retardation corrections. We plotted the effective potentials with and without retardation corrections in Figure 2: the height, its location and the curvature of the potential at the top of the barrier vary strongly when one compares the two set of effective potentials (see Table 2).

Table 2. Parameters for the curves of Figure 2. For a given value of C_0, there are two potential curves, $V_{\rm exact}$ (with retardation) and $V_{\rm noret}$ (without retardation). We give the height of the potential $V_{\rm max}$, the corresponding velocity $v_{\rm top}$, ($V_{\rm max} = \frac{1}{2}mv_{\rm top}^2$), the location of the maximum of the barrier $z_{\rm max}$, and the curvature $\alpha = \partial^2 V/\partial z^2\big|_{z=z_{\rm max}}$ at the top of the barrier. For $V_{\rm noret}$ of Figures 2e and 2f, there is no barrier.

Figure	C_0 (10^{-10} a.u.)	type	$V_{\rm max}$ (10^{-11} a.u.)	$v_{\rm top}$ (cm/s)	$z_{\rm max}$ (a_0)	α (10^{-16} a.u.)
2a	9.877	exact	13.454	17.53	1629.5	–3.7754
		no ret.	4.378	10.00	2243.4	–1.0531
2b	7.463	exact	8.207	13.69	1793.0	–2.1277
		no ret.	1.576	6.00	2614.9	–0.4077
2c	6.023	exact	5.483	11.19	1935.2	–1.3649
		no ret.	0.394	3.00	3022.2	–0.1542
2d	5.375	exact	4.378	10.00	2017.5	–1.0541
		no ret.	0.013	0.54	3334.6	–0.0739
2e	3.391	exact	1.576	6.00	2416.9	–0.3447
		no ret.	–	–	–	–
2f	2.119	exact	0.394	3.00	3000.4	–0.0828
		no ret.	–	–	–	–

2.4 Quantum reflection and tunneling

Classically, a particle of mass m and velocity v (momentum $\hbar k = mv$) incident on a one dimensional potential barrier $V(z)$ can be either transmitted or reflected; the classical reflection probability is a Heavyside function $\mathsf{R}_{\rm classic}(E) \equiv \Theta(V_{\rm max} - E)$, where $E = \frac{1}{2}mv^2$ is the energy of the atom and $V_{\rm max} = \max[V(z)]$ is the height of the potential barrier. In quantum mechanics the reflection probability $\mathsf{R}(E)$ is a smooth function of the energy: the classical step-function is replaced by a quantum S-shaped curve, with a finite overbarrier reflection probability as well as a finite underbarrier transmission (or tunneling) probability.

The reflection probability for an arbitrary potential is evaluated as in [31]; the procedure is based on matching a superposition of incoming and reflected Wentzel-Kramers-Brillouin (WKB) waves to an exact or accurate approximate solution of the Schrödinger equation bridging the region where the WKB approximation is inaccurate. For quantum reflection (or above barrier) to occur, the WKB approximation must be violated. This observation offers a simple way to optimize laser parameters for quantum reflection, based on the concept of "badlands" [29–31], a notion introduced to quantify the extent to which WKB is violated for a given energy of the incoming atoms at each coordinate z. The essential condition for applicability of the WKB approximation is that the de Broglie wavelength $\lambda_{dB} = 2\pi\hbar/p$, with $p(E,z) = \sqrt{2m[E - V(z)]}$, varies

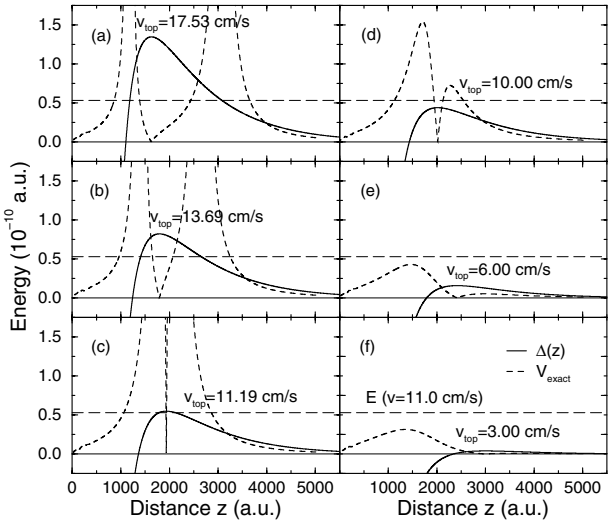

Fig. 3. The dimensionless badlands $\Delta(z)$ (dashed lines) for the exact potentials $V_{\rm exact}$ of the Figure 2 (solid line), for an incoming atom with $E = 5.2975\times10^{-11}$a.u. (or $v = 11.0$ cm/s). The potential $V_{\rm exact}$ and energy E (the horizontal dashed line) are on a scale of 10^{-10}a.u., and the badlands on a unit scale. (a), (b) and (c) correspond to tunneling through the barrier (the classical turning points are indicated by the intersection of E with $V_{\rm exact}$) and (d), (e) and (f) represent the above barrier cases.

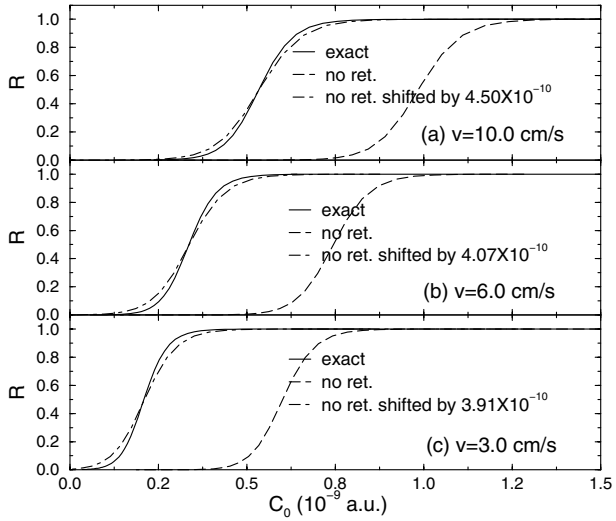

Fig. 4. Comparison of the reflection probability $\mathsf{R}(E)$ as a function of C_0 for $V_{\rm exact}$ and $V_{\rm noret.}$, at three different incident velocities: 10.0 cm/s in (a), 6.0 cm/s in (b), and 3.0 cm/s in (c). Near the classical threshold $C_0 = C^{\rm classic}$, ($V_{\rm max} = E$), R increases from zero to one. These thresholds are shifted by the retardation effects. The shift, given in each plot in a.u., is larger for a higher velocity. The S-shape of the curve results from quantum effects and is also sensitive to retardation. As v is decreased, this S-shape becomes steeper. To illustrate the variation in shape, with and without retardation, we shift the curves without retardation by the differences in $C^{\rm classic}$.

sufficiently slowly,

$$\Delta(z) \equiv \frac{1}{2\pi}\left|\frac{d\lambda_{dB}}{dz}\right| = \hbar\left|\frac{m}{p^3}\frac{dV}{dz}\right| \ll 1. \qquad (8)$$

The "badlands" are the regions where the condition (8) is not fulfilled and the "badness" is Δ. Alternative definitions for the badlands are also useful [32,33]. Note that the badlands are determined by both the potential and the energy. The stronger and wider are the badlands, the larger is the quantum reflection.

Experiments can be performed in two distinct ways; by keeping the intensity of the laser constant and changing the energy of the incoming atoms, or by keeping a constant energy and varying the intensity of the laser. We computed and compared the reflection probability $\mathsf{R}(E)$ for $V_{\rm exact}$ and $V_{\rm noret}$ for both approaches. We found that by varying the velocity of the incoming atoms (for a constant intensity), the difference in the shape of $\mathsf{R}(E)$ being extremely small so that only a threshold change could be measured [30]. For a constant velocity, by varying the intensity of the laser (or equivalently C_0), we change the shape and extent of the barrier; as C_0 is decreased, the barrier is lowered and moved out (see Fig. 2). By doing so, one probes different regions of the atom-wall potential. The results of calculations for incoming atoms with velocities of 3.0, 6.0 and 10.0 cm/s are presented in Figure 4. In order to quantify both above barrier reflection and quantum tunneling, we define the areas A_1 and A_2 (see Fig. 5) for $\mathsf{R}(E)$ as a function of C_0. As illustrated in Table 3 below, retardation has an effect of nearly 25% on A_1 and A_2 at $v = 3.0$ cm/s.

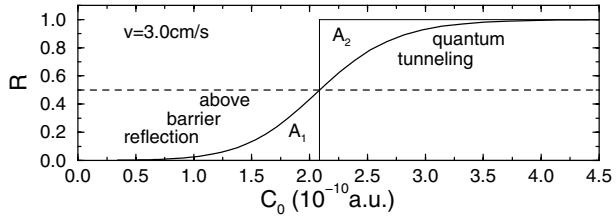

Fig. 5. A reflection probability curve of $\mathsf{R}(E)$ as a function of the laser intensity C_0. The areas A_1 and A_2 correspond to above barrier reflection and quantum tunneling, respectively, and they are defined by the vertical line cutting the curve at $\mathsf{R} = 0.5$ located (by definition) at $C_0 = C_{1/2}$.

2.5 Enhancement of quantum effects

By using more than one laser beam, it is possible to enhance quantum effects by creating "sharp" features in the effective potential $V(z)$, i.e. regions were the variation in the potential $|dV/dz|$ is larger than $p^3/m\hbar$ so that $\Delta(z)$ becomes of the order one or larger. For example, using a red-detuned in addition to the blue-detuned laser, and by selecting the appropriate incident angles, we can produce a potential that is everywhere attractive (i.e. negative) but for which the "badlands" would become quite important, leading to sizable quantum effects.

Here, we investigate a realistic system based on a bichromatic evanescent-wave setting (Fig. 6). We show below that it allows for a significant increase in above barrier reflection. Note that two colors evanescent-wave potentials

Table 3. Quantum reflection and tunneling signatures. $C_{1/2}$ and $C^{\rm classic}$ are defined in Figure 4, while A_1 and A_2 are defined in Figure 5 and represent above barrier reflection and quantum tunneling, respectively, for the curves of Figure 4. $A_1 + A_2$ are measures of the total quantum signature. For all quantities (expressed in units of 10^{-11} a.u.), we give the ratio ret./no ret. As the velocity v is reduced, the effect of retardation is more pronounced. At $v = 3$ cm/s retardation has an effect of nearly 25% on A_1 and A_2.

Quantity (10^{-11} a.u.)	type	v (in cm/s) 10.0	6.0	3.0
$C_{1/2}$	ret.	53.327	33.563	20.852
	no ret.	98.439	74.400	60.126
$C^{\rm classic}$	ret.	53.755	33.901	21.188
	no ret.	98.735	74.622	60.246
A_1	ret.	3.2350	2.6049	2.1485
	no ret.	4.0013	3.4540	2.9779
	ratio	0.8085	0.7542	0.7215
A_2	ret.	3.5009	2.8654	2.4245
	no ret.	4.2543	3.6976	3.2683
	ratio	0.8229	0.7749	0.7418
$A_1 + A_2$	ret.	6.7359	5.4703	4.5729
	no ret.	8.2556	7.1516	6.2462
	ratio	0.8159	0.7649	0.7321

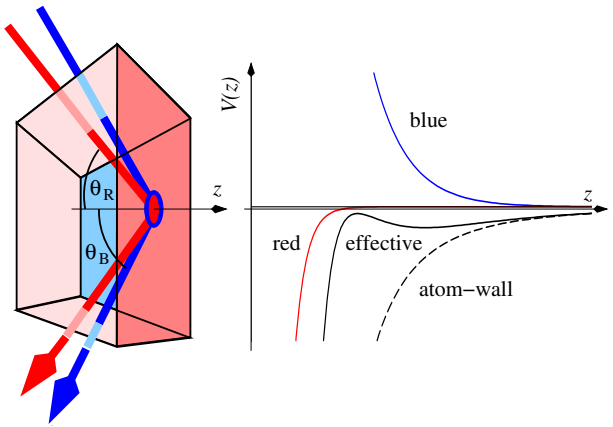

Fig. 6. Bichromatic evanescent-wave mirror. On the left panel, we show a schematic of the prism and the two lasers, defining $\theta_{\rm R}$ and $\theta_{\rm B}$. The right panel illustrates the various contributions to the effective potential $V(z)$.

[34] together with hollow laser beams were proposed [35] to create atom traps where evaporative cooling can take place [36].

The two exponentially decaying optical potentials [red (R) and blue (B) detuned] and the attractive atom-wall interaction add up to generate the effective potential:

$$V(z) = C_{\rm B} e^{-2\kappa_{\rm B} z} - C_{\rm R} e^{-2\kappa_{\rm R} z} - \frac{C_3}{z^3}, \qquad (9)$$

with $\kappa_{\rm B/R} = k_{\rm B/R}\sqrt{n^2 \sin^2\theta_{\rm B/R} - 1}$, where $\theta_{\rm B/R}$ are the incident angles of the laser beams, and $k_{\rm B/R}$ are their wave numbers. The maximum of the optical potentials at $z = 0$, $C_{\rm B/R}$, are determined by the intensity $I_{\rm B/R}$ and the detuning from the resonance $\delta_{\rm B/R}$. For large detuning, we have (as before) $C_{\rm B/R} \simeq I_{\rm B/R} d^2/8\hbar\epsilon_0\delta_{\rm B/R}$. We use here the simplest approximation for the atom-wall interaction — the Lennard-Jones potential with $C_3 = C_3^{\rm metal}(n^2-1)/(n^2+1)$. Extending our treatment to more accurate potentials, including in particular retardation effects, is straightforward. In this example, we use $n = 1.5$ and $k_{\rm B/R} = k_L$; we vary detunings and angles (all other parameters for Na atoms are given in Table 1).

We want to enhance a fully quantum effect — above barrier reflection — and so $V < 0$ for all z. For Δ to be significant, $p(E, z)$ must be small and/or dV/dz large. The various parameters are restricted by experimental constraints [37]. The incident angle must be larger than the critical angle θ_c for total reflection (here 41.8° for $n = 1.5$) and roughly smaller than 55° [37], while detunings from resonance should be detuned 1 GHz or more to avoid spontaneous emission. The intensities are typically of the order of 100 mW/mm^2. The values of $C_{\rm B}$ and $C_{\rm R}$ will be of the order of 10^{-9} a.u. (or about 6 MHz), while $\kappa_{\rm B}$ and $\kappa_{\rm R}$ will vary more wildly depending on the angles.

So, we consider incident sodium atoms with $v = 10$ cm/s. We keep the red-detuned laser beam intensity and detuning at fixed values ($I = 100$ mW/mm^2 and $\delta = 2\pi \times 1.1$ GHz), so that $C_{\rm R} = 1.3 \times 10^{-9}$ a.u. (or 8.6 MHz): the values of $C_{\rm B}$ optimizing the reflection coefficient R, labeled $C_{\rm B}^{\rm opt}$, depends on the angles of the beams [28]. We fix $\theta_{\rm B}$ at 55° (with $\kappa_{\rm B} = 4.0304 \times 10^{-4}$ a.u.), and vary $\theta_{\rm R}$ starting just above $\theta_c = 41.8°$, from 42° to 45°. The parameters are listed in Table 4, together with the corresponding reflection coefficients R. As $\theta_{\rm R}$ gets closer to θ_c, R becomes larger: for $\theta_{\rm R} = 42°$, nearly 30% of the incoming atoms will be reflected by the purely attractive interaction, a large improvement over the 0.001% value without lasers on.

The effective potential and badlands are shown in Figure 7 for the case $\theta_{\rm R} = 43°$ in Table 4: the effect of the combined evanescent-waves is drastic, creating a "sharp" structure in $V(z)$ (i.e. $|dV/dz|$ becomes larger than $p^3/m\hbar$), and driving the badlands in the regime where quantum effects are significant (i.e. $\Delta(z)$ becomes of the order one or larger). Because quantum reflection occurs mainly near Δ maximum [32,33], Figure 7 confirms our use of $-C_3/z^3$: here $\lambda/2\pi = 1772$ a.u. (Na), while Δ maximum is located near 1000 a.u., so that retardation effects can safely be neglected.

In Figure 8, we show R as a function of $C_{\rm B}$. For each angle $\theta_{\rm R}$, we obtained an S-shape for the reflection coefficient R [28–30]. Because $I_{\rm B}$ necessary to produce the feature in $V(z)$ is smaller for large angles $\theta_{\rm R}$ (see Eq. (9) and Fig. 6), S-shape curves are shifted to lower values of $C_{\rm B}$ as $\theta_{\rm R}$ increases. The shaded areas illustrate the region for which the effective potential is purely attractive, hence the corresponding reflection is purely quantal in origin. We note that these shaded regions are more extended

Table 4. Reflection coefficient R for various parameters. Here, the angle for the blue laser is fixed to 55° (or $\kappa_{\rm B} = 4.0304 \times 10^{-4}$ a.u.), while the detuning and intensity of the red laser are set to give $C_{\rm R} = 1.3 \times 10^{-9}$ a.u.

$\theta_{\rm R}$	$\kappa_{\rm R}$ (10^{-5} a.u.)	$C_{\rm B} = C_{\rm B}^{\rm opt}$ (10^{-9} a.u.)	R ($v = 10$ cm/s)
42°	4.8578	4.143	0.284
43°	12.176	3.641	0.226
44°	16.529	3.345	0.180
45°	19.958	3.112	0.142
no laser			0.000011

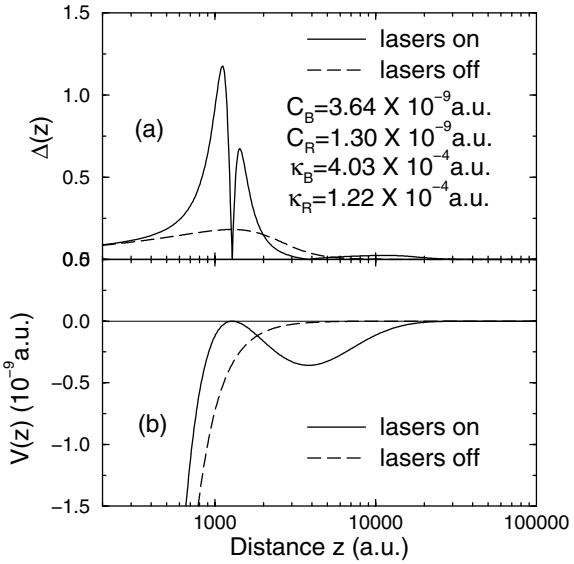

Fig. 7. Comparison of the badlands (a) and the potentials (b) when the lasers are on and off (for $\theta_{\rm R} = 43^{\rm o}$ in Table 4).

for smaller $\theta_{\rm R}$, translating the fact that R for purely quantum reflection is larger and grows more rapidly with $C_{\rm B}$ for smaller angles $\theta_{\rm R}$.

Naturally, the parameter space is much larger than what we show here, and if the experimental constraints can be relaxed, even more dramatic results can be obtained. For example, modification and control of the effective potential could be achieved by changing the detuning and intensities of the lasers in real time. Finally, one could employ many lasers to design complicated effective potentials tailored to specific tasks: the possible applications are practically unlimited.

3 Molecules

Over the last few years, rapid progress has been realized in cooling and trapping molecules (e.g., see the special issue [38] of Eur. Phys. J. D), and more recently, many groups have reported results on polar molecules, such as KRb [39–42], RbCs [43,44], NaCs [45], or LiH [46]. It is only natural to ask the question: How does a polar molecule interact with an evanescent-wave mirror?

In this section, we extend the treatment of EWM to molecules. More specifically, we describe the interaction

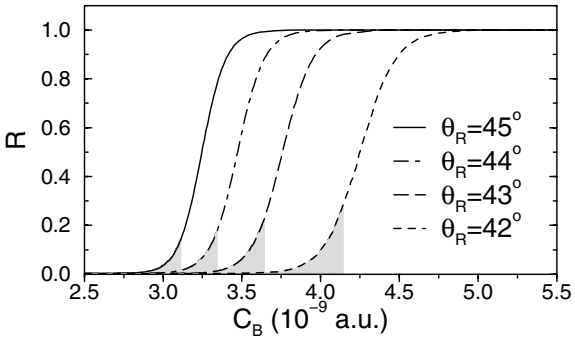

Fig. 8. Reflection coefficient as a function of $C_{\rm B}$ for various angle $\theta_{\rm R}$. Here, $C_{\rm R} = 1.3 \times 10^{-9}$ a.u. and $\theta_{\rm B} = 55^{\rm o}$. In (a), the shaded regions illustrate parameters for which the effective potential is purely attractive, corresponding to pure quantum reflection. In (b), the same R are plotted in terms of the scaled parameter $C_{\rm B}/C_{\rm B}^{\rm opt}$ on a logarithmic scale: $C_{\rm B}/C_{\rm B}^{\rm opt} < 1$ corresponds to pure quantum reflection.

of a polar diatomic molecule with a EWM. We consider a diatomic molecule in its ground vibronic (i.e. vibrational and electronic) state but with a manifold of rotational states with the quantum number J. This manifold will be coupled to another manifold of a single excited vibronic state. We concentrate our efforts on lithium hydride [46], but our treatment can directly be applied to other polar molecules being produced in today's experiments, such as LiCs, KRb, etc.

In most cases, we can choose the two electronic states to be $^1\Sigma$ states, and hence the states are fully characterized by their J and M_J quantum numbers. The model is presented here in several stages. First we define our system of coordinates and some physical considerations. Then we describe separately the interaction of the molecule with the evanescent wave from the laser light and with the wall. We then combine both and obtain the dynamical coupled equations for the system. We solve them using a time-dependent approach (as opposed to the time-independent treatment for atoms presented in the previous section), and comment on the resulting simulations.

3.1 Coordinates and method

In Figure 9, we define the coordinates for the molecular EWM system. The molecular center of mass is placed in a distance z from the prism. The light can be linearly or circularly polarized with respect to some y-direction perpendicular to the z-axis. The angles θ and ϕ are the two rotational angles of the molecule and its dipole $\vec{\mu}$ with respect to the y-axis. The angle η is the angle of incidence of the light normal to the prism, and the evanescent light intensity is given by: $I(z) = I(0)\exp(-2\kappa z)$, where $\kappa = k\sqrt{n^2 \sin^2 \eta - 1}$, k is the wavevector of the light, and n is the index of refraction of the media. The internal states of the molecule are given by:

$$|e, v, J, M, \Lambda\rangle = \sqrt{\frac{2J+1}{4\pi}}\psi_v(R)D^J_{-M,-\Lambda}|e\rangle. \qquad (10)$$

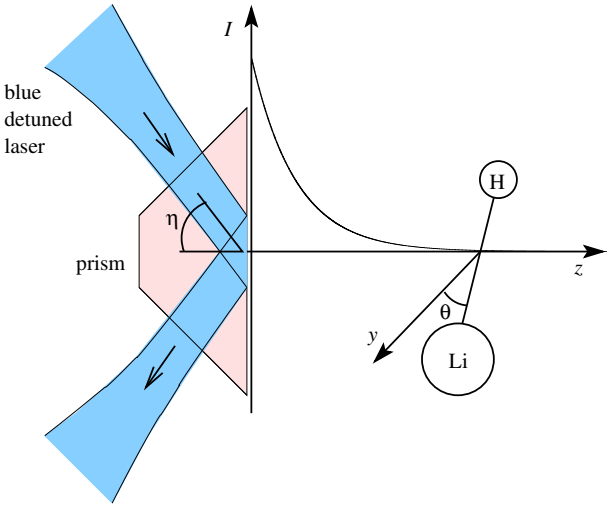

Fig. 9. Experimental set-up for the molecular EWM. A blue detuned laser light enters a prism of index of refraction n with angle η. The evanescent part of the light creates an exponentially decaying wave which interacts with the diatomic molecule with a dipole moment $\vec{\mu}$ at a distance z from the prism. θ and ϕ are the angles between the molecular axis and the direction of the polarization of the light.

Here, e and v are the electronic and the vibrational quantum numbers, respectively, and Λ is the projection of the electronic angular momentum on the molecular axis. The vibrational wavefunction $\psi_v(R)$ depends on the internuclear separation R, and $D^J_{M,\Lambda}$ is a tensor of rank J for the transformation of the rotation matrices.

We can now move to the task of writing the potentials being exerted on the various internal states of the molecule as a function of the internal molecular degrees of freedom. Dynamical equations for the external motion of the molecules will be obtained by taking the taking the trace to eliminate these degrees of freedom.

3.2 Molecule-light interaction

The interaction of the molecule with light is described by $-\vec{\mu}\cdot\vec{E}$, where $\vec{E}$ is the electric field. We relate the components of the dipole moment μ_q in the molecule-fixed frame to component in the space-fixed frame μ_p ($p=0,\pm1$ for light with linear and circular polarization, respectively) using the relations [47]

$$\mu_p = \sum_q D^{1*}_{p,q}\mu_q = \sum_q (-1)^{p,-q} D^1_{-p,-q}\mu_q. \tag{11}$$

The interaction between two ro-vibrational states with light of a certain polarization p is given by [48,49]:

see equation (12) below.

Here, μ^t_q is the transition dipole moment between two vibronic states, $E_p(z)$ is the space dependent electric field for the polarization p, and we employ Wigner 3-j symbols [47,49,50]. The angles θ, ϕ, and χ are the Euler angles corresponding to the rotation of a general rigid rotor; although only θ and ϕ are required for a linear molecule, χ is necessary in general. The single component of μ_q that contributes to the transition is determined by $q=\Lambda-\Lambda'$. In the rest of this paper, we assume a linearly polarized light, so that the light does not couple between states with different M. This simplifies our treatment, but the results for other type of polarization can be derived in a straight forward manner.

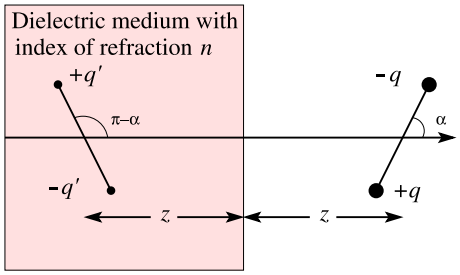

Fig. 10. Dipole and its image in a dielectric medium.

3.3 Molecule-Wall Interaction

For our purpose, we can model the molecule by a classical dipole moment, and use the electrostatic image method to derive the interaction of a dipole in a vicinity of an infinite dielectric wall [51], as drawn in Figure 10. The dipole $\vec{\mu}$ is at the point $x_0=(0,0,z)$ from the wall, the angle between the dipole and the z axis is α, and the magnitude of the dipole is given by $|\mu|$. The image dipole $\vec{\mu}'$ is placed at

$$\begin{aligned}
\frac{\hbar}{2}\Omega^{e,v,J,M,\Lambda}_{e',v',J',M',\Lambda'} &= -E_p(z)\langle e',v',J',M',\Lambda'|\mu_p|e,v,J,M,\Lambda\rangle\ , \\
&= -E_p(z)\sum_q \langle e',v',J',M',\Lambda'|D^{1*}_{p,q}\mu_q|e,v,J,M,\Lambda\rangle\ , \\
&= -E_p(z)\frac{1}{4\pi}\sqrt{(2J+1)(2J'+1)}\sum_q (-1)^{M-\Lambda+p-q}\langle e',v'|\mu_q|e,v\rangle\int D^{J'*}_{M',\Lambda'}D^1_{-p,-q}D^J_{-M,-\Lambda}d\theta d\phi d\chi\ , \\
&= -E_p(z)\sqrt{\frac{2J'+1}{2J+1}}\sum_q (-1)^{M-\Lambda+p-q}\mu^t_q \begin{pmatrix} J & 1 & J' \\ -M & p & M'\end{pmatrix}\begin{pmatrix} J & 1 & J' \\ -\Lambda & -q & \Lambda'\end{pmatrix}
\end{aligned} \tag{12}$$

$$\begin{pmatrix}
V_{0,0}^{0,0} & 0 & 0 & 0 & 0 & 0 & 0 & 0 & 0 \\
0 & V_{1,-1}^{1,-1}+B & 0 & V_{1,1}^{1,-1} & 0 & 0 & 0 & 0 & 0 \\
0 & 0 & V_{1,0}^{1,0}+B & 0 & 0 & 0 & 0 & 0 & 0 \\
0 & V_{1,1}^{1,-1} & 0 & V_{1,1}^{1,1}+B & 0 & 0 & 0 & 0 & 0 \\
0 & 0 & 0 & 0 & V_{2,-2}^{2,-2}+3B & 0 & V_{2,0}^{2,-2} & 0 & 0 \\
0 & 0 & 0 & 0 & 0 & V_{2,-1}^{2,-1}+3B & 0 & V_{2,1}^{2,-1} & 0 \\
0 & 0 & 0 & 0 & V_{2,0}^{2,-2} & 0 & V_{2,0}^{2,0}+3B & 0 & V_{2,2}^{2,0} \\
0 & 0 & 0 & 0 & 0 & V_{2,1}^{2,-1} & 0 & V_{2,1}^{2,1}+3B & 0 \\
0 & 0 & 0 & 0 & 0 & 0 & V_{2,2}^{2,0} & 0 & V_{2,2}^{2,2}+3B
\end{pmatrix} . \tag{21}$$

$x_0' = (0, 0, -z)$, the angle between the dipole and the z-axis is $\pi - \alpha$, and its magnitude is to be determined from the appropriate boundary conditions. The field for $z > 0$ is given by:

$$\vec{E}_{z>0}(\vec{x}) = \frac{3\vec{n}(\vec{\mu}\cdot\vec{n}) - \vec{\mu}}{|\vec{x}-\vec{x}_0|^3} + \frac{3\vec{n}'(\vec{\mu}'\cdot\vec{n}') - \vec{\mu}'}{|\vec{x}-\vec{x}_0'|^3} , \tag{13}$$

where $\vec{n}$ and $\vec{n}'$ are unit vectors on the direction from $\vec{x}$ to $\vec{x}_0$ and $\vec{x}_0'$, respectively. The field for $z < 0$ results from an effective dipole identical to $\vec{\mu}$ in its position and direction, but with a magnitude b to be determined by the boundary conditions. The field is then given by:

$$\vec{E}_{z<0}(\vec{x}) = \frac{3\vec{n}(b\vec{\mu}\cdot\vec{n}) - b\vec{\mu}}{|\vec{x}-\vec{x}_0|^3} . \tag{14}$$

The boundary conditions for this geometry are:

$$\lim_{z\to 0^+} E_\parallel = \lim_{z\to 0^-} E_\parallel , \tag{15a}$$

$$\lim_{z\to 0^+} E_\perp = \lim_{z\to 0^-} n^2 E_\perp . \tag{15b}$$

Substituting equations (13) and (14) into equations (15) gives

$$|\vec{\mu}'| = \frac{1-n^2}{1+n^2} , \tag{16a}$$

$$b = \frac{2n^2}{n^2+1} , \tag{16b}$$

so that the potential energy for a dipole near the dielectric media is given by

$$\begin{aligned} V_e(z) &= -\left(\frac{n^2-1}{n^2+1}\right)\frac{|\mu_e|^2}{16z^3}(1+\cos^2\alpha) , \\ &= -\frac{C_e}{z^3}[1 + (1-\cos^2\theta)\sin^2\phi] , \end{aligned} \tag{17}$$

with $C_e \equiv [(n^2-1)/(n^2+1)](|\vec{\mu}_e|^2/16)$, where $\vec{\mu}_e = \langle e, v|\vec{\mu}|e, v\rangle$ is the dipole moment for the electronic state e. Here θ and ϕ are the space-fixed rotational angles with respect to the y-axis, defined above. The interaction depends only on the rotational degree of freedom of the molecule, and the coupling between two rotational states within a certain vibronic state is given by:

$$V_{J,M}^{J',M'}(z) = -\frac{C_e}{z^3}\langle J', M'|1 + (1-\cos^2\theta)\cos^2\varphi|J, M\rangle. \tag{18}$$

The spherical harmonics $Y_M^J(\theta,\phi)$ satisfy the identity

$$\cos\theta Y_M^J = j_M^{J+1} Y_M^{J+1} + j_M^J Y_M^{J-1} , \tag{19}$$

where $j_M^J = \sqrt{(J^2-M^2)/(4J^2-1)}$. The coupling between two rovibronic states is restricted by the selection rules $\Delta J = 0, \pm 2$, $\Delta M = 0, \pm 2$, and is given by:

$$\begin{aligned} V_{e',v',J',M'}^{e,v,J,M}(z) = -\frac{C_e}{z^3}\Bigg[&\delta_J^{J'}\delta_M^{M'} + \Big(\delta_J^{J'} - j_{J'+1}^{M'} j_{J+1}^{M}\delta_{J'+1}^{J+1} \\ &- j_{J'+1}^{M'} j_J^M \delta_{J'+1}^{J-1} - j_{J'}^{M'} j_{J+1}^{M}\delta_{J'-1}^{J+1} - j_{J'}^{M'} j_J^M \delta_{J'-1}^{J-1}\Big) \\ &\times \left(\frac{\delta_M^{M'}}{2} + \frac{\delta_M^{M'+2} + \delta_M^{M'-2}}{4}\right)\Bigg]. \end{aligned} \tag{20}$$

Note that while all the diagonal terms are attractive, some of the off-diagonal terms result in repulsive coupling potentials. In addition, the coupling between two states with different J's is non-vanishing only for states with $|M| < J$.

3.4 Combined potential and dynamical equations

Substituting the relations derived in the previous two sections into the full Hamiltonian, we obtain a matrix made of four blocks, two diagonal blocks which involve interaction within a single electronic state, and two off-diagonal interaction blocks, which contain the molecule-light interaction. As an example, we consider only the coupling between the various rotational states of the ground electronic $v = 0$ vibrational state, and adopt the simplified notation $V_{J',M'}^{J,M} \equiv V_{g,v=0,J',M'}^{g,v=0,J,M}$. Using a dressed state picture, the block of the interaction within the ground electronic state up to $J = 2$ is given by:

see equation (21) above.

Here $B \equiv 2B_0$, where B_0 is the rotational constant for the ground electronic state. The corresponding block for the excited electronic state will have the same form, with additional diagonal detuning term $\hbar\Delta$, and with B_0 begin replaced by B_1. We assume a linearly polarized light, and the off-diagonal blocks $\frac{\hbar}{2}\tilde{\Omega}$ will be two hermitian conjugate

with the matrix $\tilde{\Omega}$ of the form:

$$\begin{pmatrix} 0 & 0 & \Omega_{0,0}^{1,0} & 0 & 0 & 0 & 0 & 0 & 0 \\ 0 & 0 & 0 & 0 & 0 & \Omega_{1,-1}^{2,-1} & 0 & 0 & 0 \\ \Omega_{0,0}^{1,0} & 0 & 0 & 0 & 0 & 0 & \Omega_{1,0}^{2,0} & 0 & 0 \\ 0 & 0 & 0 & 0 & 0 & 0 & 0 & \Omega_{1,1}^{2,1} & 0 \\ 0 & 0 & 0 & 0 & 0 & 0 & 0 & 0 & 0 \\ 0 & \Omega_{1,-1}^{2,-1} & 0 & 0 & 0 & 0 & 0 & 0 & 0 \\ 0 & 0 & \Omega_{1,0}^{2,0} & 0 & 0 & 0 & 0 & 0 & 0 \\ 0 & 0 & 0 & \Omega_{1,1}^{2,1} & 0 & 0 & 0 & 0 & 0 \\ 0 & 0 & 0 & 0 & 0 & 0 & 0 & 0 & 0 \end{pmatrix}.$$

Now, we can choose an excited electronic state such that $\mu_e \ll \mu_g$, and then, using the fact that the light intensity is very low (at the order of W/cm^2 or less), we can adiabatically eliminate the upper vibronic state manifold of states, i.e. set $-i\hbar\partial_t |e, J, M\rangle = 0$, and get for the upper manifold:

$$|J, \pm J\rangle_e = -\frac{\hbar}{2}\frac{\Omega_{J,\pm J}^{J,\pm J}|J+1, \pm J\rangle}{\hbar\Delta + J(J+1)B_1}\,, \tag{22}$$

for the case $|M| = J$, and:

$$|J, M\rangle_e = -\frac{\hbar}{2}\frac{\Omega_{J,M}^{J-1,M}|J-1, M\rangle + \Omega_{J,M}^{J+1,M}|J+1, M\rangle}{\hbar\Delta + J(J+1)B_1}\,, \tag{23}$$

for $|M| < J$. We can then substitute these expressions into the equations for the ground vibronic manifold and obtain the following dynamical equations

$$-i\hbar\partial_t|0,0\rangle = \left(\hat{T} + V_{0,0}^{0,0}\right)|0,0\rangle - \frac{\hbar^2}{4}\frac{\left|\Omega_{1,0}^{0,0}\right|^2|0,0\rangle + \Omega_{1,0}^{0,0}\Omega_{1,0}^{2,0}|2,0\rangle}{\hbar\Delta + 2B_1}\,, \tag{24}$$

$$-i\hbar\partial_t|1,\pm1\rangle = \left(\hat{T} + 2B_1 + V_{1,\pm1}^{1,\pm1}\right)|1,\pm1\rangle + V_{1,\pm1}^{1,\mp1}|1,\mp1\rangle - \frac{\hbar^2}{4}\frac{\left|\Omega_{2,\pm1}^{1,\pm1}\right|^2|1,\pm1\rangle + \Omega_{2,\pm1}^{1,\pm1}\Omega_{2,\pm1}^{3,\pm1}|3,\pm1\rangle}{\hbar\Delta + 6B_1}\,, \tag{25}$$

$$-i\hbar\partial_t|1,0\rangle = \left(\hat{T} + 2B_1 + V_{1,0}^{1,0}\right)|1,0\rangle + V_{1,0}^{3,0}|3,0\rangle - \frac{\hbar^2}{4}\frac{\left|\Omega_{2,0}^{1,0}\right|^2|1,0\rangle + \Omega_{2,0}^{1,0}\Omega_{2,0}^{3,0}|3,0\rangle}{\hbar\Delta + 6B_1} - \frac{\hbar^2}{4}\frac{\left|\Omega_{1,0}^{0,0}\right|^2|1,0\rangle}{\hbar\Delta}\,, \tag{26}$$

$$-i\hbar\partial_t|2,\pm2\rangle = \left(\hat{T} + 6B_1 + V_{2,\pm2}^{2,\pm2}\right)|2,\pm2\rangle + V_{2,\pm2}^{2,0}|2,0\rangle - \frac{\hbar^2}{4}\frac{\left|\Omega_{3,\pm2}^{2,\pm2}\right|^2|2,\pm2\rangle + \Omega_{3,\pm2}^{2,\pm2}\Omega_{3,\pm2}^{4,\pm2}|4,\pm2\rangle}{\hbar\Delta + 12B_1}\,, \tag{27}$$

$$\begin{aligned}-i\hbar\partial_t|2,\pm1\rangle = &\left(\hat{T} + 6B_1 + V_{2,\pm1}^{2,\pm1}\right)|2,\pm1\rangle + V_{2,\pm1}^{2,\mp1}|2,\mp1\rangle + V_{2,\pm1}^{4,\pm1}|4,\pm1\rangle + V_{2,\pm1}^{4,\pm3}|4,\pm3\rangle + V_{2,\pm1}^{4,\mp1}|4,\mp1\rangle \\ &+\frac{\hbar^2}{4}\frac{\left|\Omega_{1,\pm1}^{2,\pm1}\right|^2|2,\pm1\rangle}{\hbar\Delta + 2B_1} + \frac{\hbar^2}{4}\frac{\left|\Omega_{3,\pm1}^{2,\pm1}\right|^2|2,\pm1\rangle + \Omega_{3,\pm1}^{2,\pm1}\Omega_{3,\pm1}^{4,\pm1}|4,\pm1\rangle}{\hbar\Delta + 12B_1}\,,\end{aligned} \tag{28}$$

$$\begin{aligned}-i\hbar\partial_t|2,0\rangle = &\left(\hat{T} + 6B_1 + V_{2,0}^{2,0}\right)|2,0\rangle + V_{2,+2}^{2,+2}|2,2\rangle + V_{2,-2}^{2,-2}|2,-2\rangle + V_{2,\pm1}^{4,\pm1}|4,\pm1\rangle + V_{2,0}^{4,0}|4,0\rangle + V_{2,+2}^{4,+2}|4,+2\rangle \\ &+V_{2,-2}^{4,-2}|4,-2\rangle + \frac{\hbar^2}{4}\frac{\left|\Omega_{1,0}^{2,0}\right|^2|2,0\rangle + \Omega_{1,0}^{2,0}\Omega_{1,0}^{0,0}|0,0\rangle}{\hbar\Delta + 2B_1} + \frac{\hbar^2}{4}\frac{\left|\Omega_{2,0}^{3,0}\right|^2|2,0\rangle + \Omega_{3,0}^{2,0}\Omega_{3,0}^{4,0}|4,0\rangle}{\hbar\Delta + 12B_1}\,.\end{aligned} \tag{29}$$

In general, for general $J > 2$, there are four cases:
(1) $|M| = J$:

$$\begin{aligned}-i\hbar\partial_t|J,\pm J\rangle = &\left(\hat{T} + J(J+1)B_1 + V_{J,\pm J}^{J,\pm J}\right)|J,\pm J\rangle + V_{J,\pm J}^{J,\pm(J-2)}|J,\pm(J-2)\rangle \\ &-\frac{\hbar^2}{4}\frac{\left|\Omega_{J,\pm J}^{J+1,\pm J}\right|^2|J,\pm J\rangle + \Omega_{J,\pm J}^{J+1,\pm J}\Omega_{J+1,\pm J}^{J+2,\pm J}|J+2,\pm J\rangle}{\hbar\Delta + (J+2)(J+1)B_1},\end{aligned} \tag{30}$$

(2) $|M| = J-1$:

$$\begin{aligned}-i\hbar\partial_t|J,\pm(J-1)\rangle = &\left(\hat{T}+J(J+1)B_1+V_{J,\pm(J-1)}^{J,\pm(J-1)}\right)|J,\pm(J-1)\rangle + V_{J,\pm(J-1)}^{J,\pm(J-3)}|J,\pm(J-3)\rangle\\ &+V_{J,\pm(J-1)}^{J-2,\pm(J-3)}|J-2,\pm(J-3)\rangle + V_{J,\pm(J-1)}^{J+2,\pm(J-1)}|J+2,\pm(J-1)\rangle\\ &+V_{J,\pm(J-1)}^{J+2,\pm(J-3)}|J+2,\pm(J-3)\rangle + V_{J,\pm(J-1)}^{J+2,\pm(J+1)}|J+2,\pm(J+1)\rangle\\ &-\frac{\hbar^2}{4}\frac{\left|\Omega_{J,\pm(J-1)}^{J+1,\pm(J-1)}\right|^2|J,\pm(J-1)\rangle+\Omega_{J,\pm(J-1)}^{J+1,\pm(J-1)}\Omega_{J+1,\pm(J-1)}^{J+2,\pm(J-1)}|J+2,\pm(J-1)\rangle}{\hbar\Delta+(J+2)(J+1)B_1}\\ &-\frac{\hbar^2}{4}\frac{\left|\Omega_{J,\pm(J-1)}^{J-1,\pm(J-1)}\right|^2|J,\pm(J-1)\rangle}{\hbar\Delta+J(J-1)B_1}\,,\end{aligned} \tag{31}$$

(3) $|M| = J-2$:

$$\begin{aligned}-i\hbar\partial_t|J,\pm(J-2)\rangle = &\left(\hat{T}+J(J+1)B_1+V_{J,\pm(J-2)}^{J,\pm(J-2)}\right)|J,\pm(J-2)\rangle + V_{J,\pm(J-2)}^{J,\pm J}|J,\pm J\rangle + V_{J,\pm(J-2)}^{J,\pm(J-4)}|J,\pm(J-4)\rangle\\ &+V_{J,\pm(J-2)}^{J-2,\pm(J-4)}|J-2,\pm(J-4)\rangle + V_{J,\pm(J-2)}^{J+2,\pm(J-2)}|J+2,\pm(J-2)\rangle + V_{J,\pm(J-2)}^{J+2,\pm J}|J+2,\pm J\rangle\\ &-\frac{\hbar^2}{4}\frac{\left|\Omega_{J,\pm(J-2)}^{J-1,\pm(J-2)}\right|^2|J,\pm(J-2)\rangle+\Omega_{J,\pm(J-2)}^{J-1,\pm(J-2)}\Omega_{J-1,\pm(J-2)}^{J-2,\pm(J-2)}|J-2,\pm(J-2)\rangle}{\hbar\Delta+J(J-1)B_1}\\ &-\frac{\hbar^2}{4}\frac{\left|\Omega_{J,\pm(J-2)}^{J+1,\pm(J-2)}\right|^2|J,\pm(J-2)\rangle+\Omega_{J,\pm(J-2)}^{J+1,\pm(J-2)}\Omega_{J+1,\pm(J-2)}^{J+2,\pm(J-2)}|J+2,\pm(J-2)\rangle}{\hbar\Delta+(J+2)(J+1)B_1}\,,\end{aligned} \tag{32}$$

(4) For all other M:

$$\begin{aligned}-i\hbar\partial_t|J,M\rangle = &\left(\hat{T}+J(J+1)B_1+V_{J,M}^{J,M}\right)|J,M\rangle + V_{J,M}^{J,M+2}|J,M+2\rangle + V_{J,M}^{J,M-2}|J,M-2\rangle + V_{J,M}^{J-2,M}|J-2,M\rangle\\ &+V_{J,M}^{J-2,M-2}|J-2,M-2\rangle + V_{J,M}^{J-2,M+2}|J-2,M+2\rangle + V_{J,M}^{J+2,M}|J+2,M\rangle + V_{J,M}^{J+2,M-2}|J+2,M-2\rangle\\ &+V_{J,M}^{J+2,M+2}|J+2,M+2\rangle - \frac{\hbar^2}{4}\frac{\left|\Omega_{J,M}^{J-1,M}\right|^2|J,M\rangle+\Omega_{J,M}^{J-1,M}\Omega_{J-1,M}^{J-2,M}|J-2,M\rangle}{\hbar\Delta+J(J-1)B_1}\\ &-\frac{\hbar^2}{4}\frac{\left|\Omega_{J,M}^{J+1,M}\right|^2|J,M\rangle+\Omega_{J,M}^{J+1,M}\Omega_{J+1,M}^{J+2,M}|J+2,M\rangle}{\hbar\Delta+(J+2)(J+1)B_1}\,.\end{aligned} \tag{33}$$

Note that there is no mixing between states with odd and even J. In Figures 11 and 12, we present separately the coupling schemes between the odd and even states for the EWM system, respectively. Despite this very complicated interaction picture, we can tune the light frequency so it couples only one pair of J levels, e.g., $\hbar\Delta \approx -2B_1$ couples only $J=0$ and $J=2$. In that case, we can prepare our system to initially occupy only these two levels and then have an effective six level system. Moreover, because the states with $M \neq 0$ are not coupled by the light, the potentials for these states are purely attractive (since $C_e < 0$), and molecules in these states will undergo perfect sticking to the surface of the prism (unless extremely slow so that significant quantum reflection occurs [7]). We can treat these populations as a loss and simulate only the two remained levels.

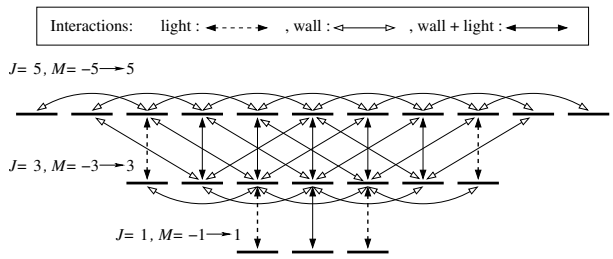

Fig. 11. Interaction scheme for states with odd J numbers. States with $J = 1, 3$, and 5 are presented.

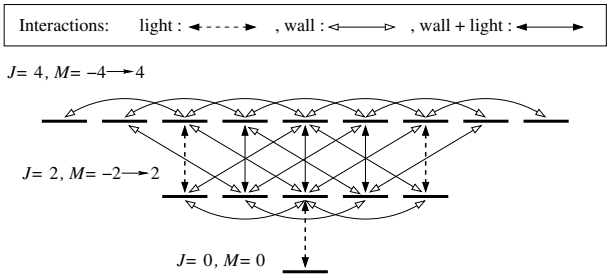

Fig. 12. Interaction scheme for states with even J numbers. States with $J = 0, 2$, and 4 are presented.

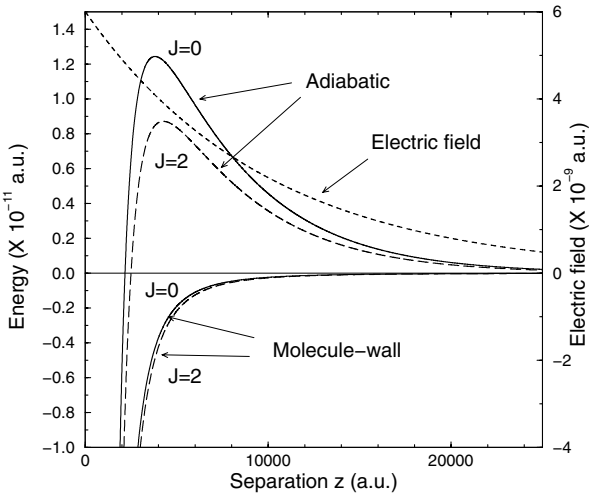

Fig. 13. Adiabatic and molecular-light potentials for $J = 0$ and $J = 2$. Also shown is the exponentially decaying electric field. See text for details regarding the physical parameters.

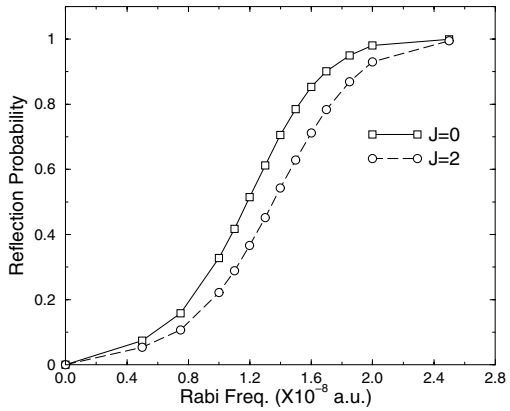

Fig. 14. Reflection probability as a function of the Rabi frequency $2\Omega_0^1(z=0)$ for $J = 0$ and 2.

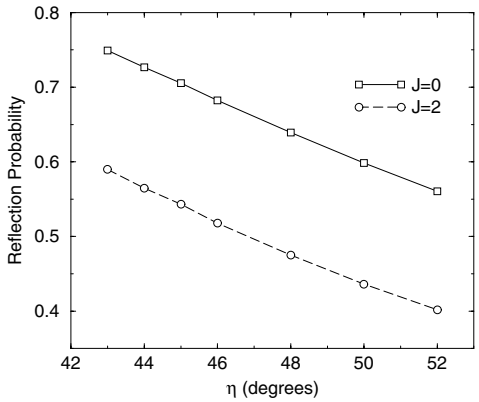

Fig. 15. Reflection probability as a function of the incident angle η for $J = 0$ and 2 with $2\Omega_0^1(z=0) = 1.5 \times 10^{-8}$ a.u.

3.5 Results

As an example we take LiH, a molecule with a large dipole moment and well-known spectroscopic parameters [48]. We took the laser frequency to be slightly detuned from the $A^1\Sigma^+ \rightarrow X^1\Sigma^+$ transition so that: $\hbar\Delta + 2B_1 = -1 \times 10^{-6}$ a.u. $= -0.2$ cm^{-1} ($|\mu_e|$ for the excited state and therefore V_e is very small compared with these energy scales), and $n = 1.8$. In Figure 13, we present two adiabatic potentials corresponding to $J = 0$ and 2 states at $z \rightarrow +\infty$ for $2\Omega_0^1(z=0) = 1.4 \times 10^{-9}$ a.u., and the corresponding molecule-wall potentials. The potential for $J = 0(2)$ shows a maximum with $E = 5.90 \times 10^{-12}(3.94 \times 10^{-12})$ Hartree at $z = 4710(5283)$ Bohr.

To obtain the reflection probability P_J of the $J = 0$ and 2 states, we solved the time-dependent coupled Schrödinger equation by the split step method. We started the simulations with an equally weighted Gaussian wavepacket of the two J states, i.e. $|\psi\rangle = |0\rangle + |2\rangle$, with average velocity V_{mol} and velocity spread ΔV from which we defined the temperature T.

Figure 14 presents the reflection probability P_J for an incoming translational velocity of 10 cm/s vs. the light intensity for $\eta = 45°$. The initial Gaussian wave packet velocity spread corresponds to 100 nK = 2.5 cm/s. The difference between the two reflection coefficients allows for quantum state selection of 15% between the two J states. In Figure 15, we present P_J vs. the incident angle η. Both curves are almost linear with the same slope within the experimentally feasible range of angles. The decrease in η reduces the effective length of the light intensity decay and thus influences the position and energy of the maxima of the adiabatic potentials. Note that the state $|\psi\rangle = |0\rangle + |2\rangle$ is not normalized to unity, so that each component can be reflected with a probability $P_J \leq 1$, and hence $P_0 + P_2 \leq 2$ in both Figures 14 and 15.

Finally, we expect a better state selectivity as $T \rightarrow 0$ K, because then the two J states have a well-defined momentum. Consequently, for kinetic energies above the $J = 2$ but below the $J = 0$ potential barrier, one would expect a complete separation. For molecular velocity of 100 cm/s, we achieve a separation of 55% at $T = 100$ nK between the two states.

4 Conclusion

In conclusion, we have shown that one can use EWM for atoms to probe quantum effects, and even study retardation effects. In addition, we showed that it is possible to design atom optic components that optimize quantum effects, in particular above barrier reflection, by creating features in the interaction potential such that the badlands become significant. We demonstrated the scheme with a bichromatic evanescent-wave mirror. In the future, detailed studies of tunneling and resonances could be performed with this system, and because the exact shape of the potential depends on the long-range atom-wall interaction, sensitivity to retardation could be studied. The evanescent-wave setting complements recent nanofabrication approaches to quantum reflection, allowing for high reflectivity for higher incident velocities.

Finally, we extended our studies to the dynamics of an ultracold molecular EWM. We showed that it might be an interesting tool for investigating state selection in ultracold molecules and various fundamental quantum effects. These were obtained at nearly attainable experimental parameters. The observed features at less realistic conditions, i.e. colder temperatures and lower $V_{\rm mol}$, are enhanced. The cold molecules field of research is still very new, and a lot of very interesting aspects and applications of molecular EVMs are yet to be explored. As in the case of atoms, the use of time-dependent light fields and potentials will allow one to increase significantly the control of the dynamics of the system and might make molecular EWMs good new devices for trapping ultracold molecules. The possibility of manipulating quantum states with molecular EWMs in a controlled but non-unitary fashion might serve as a future tool for processing quantum information.

The authors would like to thank Harvey Gould for stimulating discussions. Support received from the United States-Israel Binational Foundation and the UConn Research Foundation are gratefully acknowledged.

References

1. R.J. Cook, R.K. Hill, Opt. Commun. **43**, 258 (1982)
2. V.I. Balykin, V.S. Letokhov, Yu.B. Ovchinnikov, A.I. Sidorov, Phys. Rev. Lett. **60**, 2137 (1988)
3. B. Segev, R. Côté, M.G. Raizen, Phys. Rev. A **56**, R3350 (1997)
4. R. Côté, B. Segev, Phys. Rev. A **67**, R41604 (2003)
5. A. Landragin, J.-Y. Courtois, G. Labeyrie, N. Vansteenkiste, C.I. Westbrook, A. Aspect, Phys. Rev. Lett. **77**, 1464 (1996)
6. F. Shimizu, Phys. Rev. Lett. **86**, 987 (2001).
7. R. Côté, B. Segev, M.G. Raizen, Phys. Rev. A **58**, 3999 (1998)
8. M. Hammes, D. Rychtarik, V. Druzhinina, U. Moslener, I. Manek-Hönninger, R. Grimm, J. Mod. Opt. **47**, 2755 (2000)
9. S.J. Wark, G.I. Opat, J. Phys. B **25**, 4229 (1992)
10. P. Domokos, T. Kiss, J. Janszky, Eur. Phys. J. D **14**, 49 (2001)
11. S.A. Schulz, H.L. Bethlem, J. van Veldhoven, J. Küpper, H. Conrad, G. Meijer, Phys. Rev. Lett. **93**, 20406 (2004)
12. D. DeMille, Phys. Rev. Lett. **88**, 67901 (2002)
13. R. Wynar, R.S. Freeland, D.J. Han, C. Ryu, D.J. Heinzen, Science **287**, 1016 (2000)
14. C.M. Dion, C. Drag, O. Dulieu, B. Laburthe Tolra, F. Masnou-Seeuws, P. Pillet, Phys. Rev. Lett. **86**, 2253 (2001)
15. G. Zinner, T. Binnewies, F. Riehle, E. Tiemann Phys. Rev. Lett. **85**, 2292 (2000)
16. M.W. Mancini, G.D. Telles, A.R.L. Caires, V.S. Bagnato, L.G. Marcassa, Phys. Rev. Lett. **92**, 133203 (2004)
17. J.D. Weinstein, R. deCarvhlho, T. Guillet, B. Friedrich, J.M. Doyle, Nature **395**, 148 (1998)
18. M.S. Elioff, J.J. Valentini, D.W. Chandler, Science **302**, 1940 (2003)
19. H.L. Bethlem, G. Berden, G. Meijer, Phys. Rev. Lett. **83**, 1558 (1999).
20. H.L. Bethlem, G. Berden, F.M.H. Crompvoets, R.T. Jongma, G. Meijer, Nature **406**, 491 (2000)
21. P.F. Barker, M.N. Shneider, Phys. Rev. A **66**, 65402 (2002)
22. C. Cohen-Tannoudji, J. Dupont-Roc, G. Grynberg, *Atom-Photon Interactions* (John Wiley & Sons, New York, 1992)
23. L.E. Lennard-Jones, Trans. Faraday Soc. **28**, 333 (1932)
24. H.B.G. Casimir, D. Polder, Phys. Rev. **73**, 360 (1948)
25. I.E. Dzyaloshinskii, E.M. Lifshitz, L.P. Pitaevskii, Adv. Phys. **10**, 165 (1961)
26. M. Marinescu, A. Dalgarno, J.F. Babb, Phys. Rev. A **55**, 1530 (1997); P. Kharchenko, J.F. Babb, A. Dalgarno, Phys. Rev. A **55**, 3566 (1997)
27. P. Kharchenko, J.F. Babb, A. Dalgarno, private communication
28. R. Côté, B. Segev, Phys. Rev. A **67**, 041604(R) (2003)
29. B. Segev, R. Côté, M.G. Raizen, Phys. Rev. A **56**, R3350 (1997)
30. R. Côté, B. Segev, M.G. Raizen, Phys. Rev. A **58**, 3999 (1998)
31. R. Côté, H. Friedrich, J. Trost, Phys. Rev. A **56**, 1781 (1997)
32. H. Friedrich, G. Jacoby, C.G. Meister, Phys. Rev. A **65**, 032902 (2002)
33. H. Friedrich, J. Trost, Phys. Rep. **397**, 359 (2004)
34. Yu.B. Ovchinnikov, S.V. Shul'ga, V.I. Balykin, J. Phys. B **24**, 3173 (1991); P. Desbiolles, J. Dalibard, Opt. Commun. **132**, 540 (1996)
35. H. Engler et al., Appl. Phys. B **67**, 709 (1998)
36. M. Hammes, D. Rychtarik, B. Engeser, H.C. Nägerl, R. Grimm, Phys. Rev. Lett. **90**, 173001 (2003); M. Hammes, D. Rychtarik, H.-C. Nägerl, R. Grimm, Phys. Rev. A **66**, 051401(R) (2002); M. Hannes, D. Rychtarik, R. Grimm, C.R. Acad. Sci. Paris IV **2**, 625 (2001)
37. M.G. Raizen, private communication
38. Eur. Phys. J. D **31**, No. 2 (2004), special issue on ultracold molecules, see references therein
39. D. Wang, J. Qi, M.F. Stone, O. Nikolayeva, B. Hattaway, S.D. Gensemer, H. Wang, W.T. Zemke, P.L. Gould, E.E. Eyler, W.C. Stwalley, Eur. Phys. J. D **31**, 165 (2004)
40. D. Wang, J. Qi, M.F. Stone, O. Nikolayeva, H. Wang, B. Hattaway, S.D. Gensemer, P.L. Gould, E.E. Eyler, W.C. Stwalley, Phys. Rev. Lett. **93**, 243005 (2004)
41. S. Kotochigova, E. Tiesinga, P.S. Julienne, Eur. Phys. J. D **31**, 189 (2004)
42. Z.T. Zemke, R. Côté, W.C. Stwalley, Phys. Rev. A **71**, 062706 (2005)
43. A.J. Kerman, J.M. Sage, S. Sainis, T. Bergeman, D. DeMille, Phys. Rev. Lett. **92**, 153001 (2004)
44. A.J. Kerman, J.M. Sage, S. Sainis, T. Bergeman, D. DeMille, Phys. Rev. Lett. **92**, 033004 (2004)
45. C. Haimberger, J. Kleinert, M. Bhattacharya, N.P. Bigelow, Phys. Rev. A **70**, 021402 (2004)
46. E. Taylor-Juarros, R. Côté, K. Kirby, Eur. Phys. J. D **31**, 213 (2004)
47. R.N. Zare, *Angular Momentum* (John Wiley, NY, 1988)
48. G. Herzberg, *Molecular Spectra and Molecular Structure: I. Spectra of Diatomic Molecules*, 2nd edn. (Van Nostrand, Princeton, 1950)
49. Y.B. Band, S. Kallush, R. Baer, Chem. Phys. Lett. **392**, 23 (2004)
50. S. Kallush, Y.B. Band, Phys. Rev. A **61**, 041401(R) (2000)
51. J. D. Jackson, *Classical Electrodynamics*, 3rd edn. (John Wiley, NY, 1999)